

## Structure and dynamics of the $\gamma$ M4 transmembrane domain of the acetylcholine receptor in lipid bilayers: insights into receptor assembly and function

RODRIGO F. M. DE ALMEIDA<sup>1,2</sup>, LUÍS M. S. LOURA<sup>2,3</sup>, MANUEL PRIETO<sup>2</sup>, ANTHONY WATTS<sup>4</sup>, ALEKSANDRE FEDOROV<sup>2</sup>, & FRANCISCO J. BARRANTES<sup>4,5</sup>

<sup>1</sup>Centro de Química e Bioquímica, Faculdade de Ciências de Lisboa, Campo Grande, Lisboa, Portugal, <sup>2</sup>Centro de Química-Física Molecular, Instituto Superior Técnico, Lisboa, Portugal, <sup>3</sup>Centro e Departamento de Química, Universidade de Évora, Rua Romão Ramalho, Évora, Portugal, <sup>4</sup>Biomembrane Structure Unit, Biochemistry Department, Oxford University, Oxford, UK, and <sup>5</sup>UNESCO Chair of Biophysics & Molecular Neurobiology and Instituto de Investigaciones Bioquímicas de Bahía Blanca, Argentina

(Received 11 January 2006; and in revised form 21 February 2006)

### Abstract

A 28-mer peptide ( $\gamma$ M4) corresponding to the fourth transmembrane segment of the nicotinic acetylcholine receptor (AChR)  $\gamma$ -subunit, with a single tryptophan residue (Trp<sup>6</sup>), was reconstituted into lipid bilayers of 1-palmitoyl-2-oleoyl-*sn*-glycero-3-phosphocholine (POPC), loaded with either high or low amounts of cholesterol, i.e., in the conjugated liquid-ordered and liquid-disordered phases, respectively, at room temperature. By making use of the Trp intrinsic fluorescence, both steady-state and time-resolved fluorescence techniques were employed, namely, red-edge excitation shift effect, decay-associated spectra (DAS), and time-resolved anisotropy. The results obtained here, together with previous studies on the same reconstituted peptide, indicate that: (i) Trp<sup>6</sup> is strongly anchored in the bilayer with a defined transverse location; (ii) the modifications in the measured DAS are related to the complex result of a self-quenching process on the decay parameters; (iii) the wobbling movement of the indole moiety of Trp<sup>6</sup> is fast but severely restricted in amplitude; and, (iv) in the liquid-ordered phase, the bilayer properties and the tilt angle of the peptide enhance peptide-peptide interactions, with the formation of peptide rich patches and possibly some anti-parallel helix-helix aggregates, showing different dynamics from that of the peptide in the liquid-disordered phase where the peptide is randomly distributed.

**Keywords:** Lipid-protein interactions, neurotransmitter receptor, transmembrane peptide dynamics, membrane, cholesterol, structure-function relationship

### Introduction

The nicotinic acetylcholine receptor (AChR) is one of the best-characterized members of the ligand-gated ion channel superfamily (see review in [1]). It is a pentamer of homologous  $\alpha_2\beta\gamma\delta$  subunits. Each subunit contains four hydrophobic segments (M1–M4), which constitute membrane-spanning domains. The M4 segment of each subunit is the transmembrane (TM) domain which is more exposed to the lipid bilayer.

Experimental evidence has reinforced the view that the function of the AChR is influenced by its lipid microenvironment [2,3]. The exact nature of the interactions between the AChR TM region and the adjacent lipids has not been clearly established.

Since the discovery of a motionally restricted layer of lipids surrounding the AChR (shell, boundary or annular lipids), this distinct region has been postulated as the likely candidate where modulation of the AChR function by lipids occurs [4].

Hydrophobic photoactivatable probes have been used to identify a periodicity of the tagged lipid-exposed residues in M4 and M3 consistent with an  $\alpha$ -helical structure [5–7]. The first atomic structure of the whole TM domain of the AChR, recently determined by cryoelectron microscopy at 4 Å-resolution, suggests that all the TM segments are helical and adopt the antiparallel  $\alpha$ -helical bundle motif [8,9]. Characterizing helix-helix interactions in well defined lipid systems containing relevant AChR TM peptides can thus give insight into the

Correspondence: Rodrigo F. M. de Almeida, Centro de Química-Física Molecular, Instituto Superior Técnico, Av. Rovisco Pais, 1049-001 Lisboa, Portugal. Fax: +351 8464455. E-mail: r.almeida@mail.ist.utl.pt

interactions relevant for assembly and structural stabilization of the whole receptor macromolecule.

However, two aspects of AChR function which are still not satisfactorily understood are: (i) a description of the dynamics of the molecule, and its relation to the structural flexibility necessary for channel activity and allosteric transitions, and (ii) the role of the lipid interface in functional control. Some reports indicate that interactions at the outermost M4 lipid-contacting ring contribute to the regulation of the gating mechanism (reviewed in [2,3]). We have recently suggested that the non-bonded interactions of the outermost M4 TM ring with the rest of the TM segments (M1-3) on the one hand, and with lipid molecules on the other, constitute the link between the structural dynamics of the channel and the lipid environment [10]. In this hypothesis, the outer ring of M4 acts as the vehicle conveying information from the lipid surroundings on the whole TM region and the M2 inner ring that lines the channel [2]. This may explain why mutations in the outer ring residues of  $\alpha$ M4,  $\beta$ M4, and  $\gamma$ M4 affect channel function [11–13] and how the lipid environment affects the stability of the functional states of the AChR [14]. It also provides a rational explanation for how several pharmacologically relevant ligands that partition into the lipid bilayer affect AChR channel function [3,9]. In this context, the study of helix dynamics and flexibility becomes important for understanding the dynamic behaviour of functional TM proteins and the role of lipids in membrane protein function in general.

Here, the AChR  $\gamma$ M4 TM peptide is reconstituted in membrane model systems (vesicles of 1-palmitoyl-2-oleoyl-*sn*-glycero-3-phosphocholine (POPC) and cholesterol [Chol]), and studied by exploiting the photophysical properties of Trp<sup>453</sup> (steady-state and time resolved fluorescence techniques). Red-edge excitation shift (REES), decay-associated spectra (DAS) and time-resolved fluorescence anisotropy are used to characterize the structure and dynamics of the  $\gamma$ M4 peptide in both Chol-rich and Chol-poor bilayer environments, revealing properties that are important to receptor function and its assembly in the endoplasmic reticulum.

## Materials and methods

### Chemicals

A peptide corresponding to the AChR TM segment  $\gamma$ M4 and the two extramembranous regions, and having the sequence N-Asp-Lys-Ala-Cys-Phe-Trp-Ile-(<sup>2</sup>H<sub>3</sub>)Ala-Leu-Leu-(1-<sup>13</sup>C)Leu-Phe-Ser-Ile-(<sup>15</sup>N)Gly-Thr-Leu-Ala-Ile-Phe-Leu-Thr-(2-<sup>13</sup>C)Gly-His-Phe-Asn-Gln-Val-C, was prepared using

conventional Fmoc synthesis (NSR Centrum, Nijmegen, Holland). The resulting peptide was deemed to be over 90% pure as determined by analytical HPLC and mass spectrometry.  $\gamma$ M4 was kept lyophilized at  $-80^{\circ}\text{C}$  until use. The lipid 1-palmitoyl-2-oleoyl-*sn*-glycero-3-phosphocholine (POPC) was purchased from Avanti Polar Lipids, Birmingham, AL, USA. Chol was purchased from Sigma (St Louis, MO, USA) and quantified using a kit for Chol determination (Roche Diagnostics, Mannheim, Germany). All other reagents were of the highest purity available. All materials were used without further purification.

### Liposome preparation

Adequate amounts of stock solutions of host lipids and peptide were mixed in a chloroform/methanol solution, dried under a stream of nitrogen and high vacuum, and suspended in buffer (20 mM HEPES, 10 mM NaCl, 0.1 mM EDTA, pH = 7.4) in order to obtain multilamellar vesicles (MLV).

A total lipid concentration of 1 mM was used in all experiments, with POPC progressively replaced by Chol along the Chol-poor liquid disordered (*l<sub>d</sub>*)/Chol-rich liquid ordered (*l<sub>o</sub>*) tie-line at room temperature taken from the phase diagram published elsewhere [15]: the composition of the *l<sub>d</sub>* phase at room temperature is 88:12, while the *l<sub>o</sub>* phase is composed of 55:45 POPC:Chol (mol:mol).

The peptide concentration was determined from the absorption spectrum ( $\epsilon = 5690 \text{ M}^{-1}\text{cm}^{-1}$  at  $\lambda = 280 \text{ nm}$  [16]). The peptide concentration was varied between 0.7 and 7 mol%. Results are shown for the lowest concentration for which there is no self-quenching in the *l<sub>d</sub>* phase [17], unless stated otherwise. Prior to the photophysical measurements, the vesicle suspensions were deoxygenated by bubbling nitrogen to prevent photo-oxidation of the unsaturated compounds.

### Absorption and fluorescence measurements

Absorption spectra were obtained in a Shimadzu UV-3101PC spectrophotometer using spectral bandwidths of 2.0 nm. Steady-state fluorescence spectra were carried out in an SLM-Aminco 8100 Series 2 spectrofluorimeter, with double excitation and emission monochromators. Emission spectra were corrected using standard emission spectra of L-Tyr and L-Trp [18], using 5 mm  $\times$  5 mm quartz cuvettes and spectral bandwidth of 2–8 nm. Excitation was always at 288 nm, except for the REES study. Polarization measurements were made using quartz Glan-Thompson prism polarizers in a single-channel detection system.

The time-resolved fluorescence instrumentation (single-photon timing technique) with picosecond resolution has been previously described [19]. Trp emission was measured at  $\lambda = 340$  nm (or at the indicated wavelength in the case of the DAS; see below) using the magic angle ( $54.7^\circ$ ) relative to the vertically polarized excitation beam produced by a frequency doubled dye laser of Rhodamine 6G ( $\lambda = 288$  nm). The fluorescence decays of the  $\gamma$ M4 peptide were obtained with an accumulation of  $\sim 10,000$  to  $\sim 20,000$  counts in the peak channel and time-scales ranging from 22 ps/channel (ld, 0.7 mol%) to 15.3 ps/channel ( $l_o$  or  $l_a$ , higher peptide concentrations). The time-resolved fluorescence anisotropies were also determined using Glan-Thompson polarizers. A cut-off filter was used in addition to the detection monochromator, to further screen scattered excitation light, resulting in a negligible number of counts obtained for blank samples (vesicles without peptide).

#### Analysis of the fluorescence intensity and anisotropy decays

Data analysis was carried out as previously described [19]. The goodness of the fit was judged from the reduced  $\chi^2$ , weighted residuals and autocorrelation plots.

The average lifetime  $\bar{\tau}$  of a fluorophore with a complex fluorescence decay described by a sum of exponentials:

$$I(t) = \sum_i \alpha_i \exp(-t/\tau_i) \quad (1)$$

is defined as (e.g., [20])

$$\bar{\tau} = \sum_i \alpha_i \tau_i^2 / \sum_i \alpha_i \tau_i \quad (2)$$

where  $\alpha_i$  are the normalized pre-exponentials (amplitudes) and  $\tau_i$  are the lifetime components. The lifetime-weighted quantum yield  $\langle \tau \rangle$  of a fluorophore is described [20] as:

$$\langle \tau \rangle = \sum_i \alpha_i \tau_i \quad (3)$$

In order to determine the DAS, intensity decays were collected for ten different emission wavelengths spanning the steady-state emission spectrum of the peptide. The ten decays were fitted simultaneously (globally analysed), with three discrete exponentials, linking the lifetimes  $\tau_i$ , considering them independent of the wavelength and allowing the pre-exponentials to float freely to obtain a set of  $\alpha_i(\lambda)$  curves. Each DAS,  $I_i(\lambda)$ , was then computed through the expression (e.g., [20]):

$$I_i(\lambda) = \frac{\alpha_i(\lambda)\tau_i I(\lambda)}{\sum_i \alpha_i(\lambda)\tau_i} \quad (4)$$

where  $I(\lambda)$  is the steady state emission spectrum. The  $\chi^2$  values obtained for each of the decays from global and from individual analyses were compared to check the adequacy of the global model. The  $\chi^2$  ratios were always  $< 1.2$ , this, among other criteria (see Results) being indicative of an appropriate statistical model.

The steady-state anisotropies,  $\langle r \rangle$ , were determined according to:

$$\langle r \rangle = \frac{I_{VV} - GI_{VH}}{I_{VV} + 2GI_{VH}} \quad (5)$$

where  $I_{ij}$  are the steady-state vertical and horizontal components of the fluorescence emission with excitation vertical ( $I_{VV}$  and  $I_{VH}$ ) and horizontal ( $I_{HV}$  and  $I_{HH}$ ) to the emission axis. The correction for orientation-dependent transmittance of the emission polarizer was determined using horizontally polarized excitation light to calculate the  $G$  factor ( $G = I_{HV}/I_{HH}$ ), and an adequate blank was subtracted from each intensity reading before the calculation of the anisotropy value.

The intensity decays of polarized light  $I_{VV}(t)$  and  $I_{VH}(t)$  were obtained with the same accumulation time. The anisotropy decay parameters (rotational correlation times,  $\phi_i$ , amplitudes,  $\beta_i$ , and residual anisotropy,  $r_\infty$ ) were determined using an iterative reconvolution non-linear least squares global analysis method fitting simultaneously to the vertically and horizontally polarized emission components, according to the expressions [21]:

$$\begin{aligned} I_{VV}(t) \otimes L(t) &= \frac{1}{3} I(t) [1 + 2r(t)] \otimes L(t) \\ I_{VH}(t) \otimes L(t) &= \frac{1}{3} I(t) [1 - r(t)] \otimes L(t) \end{aligned} \quad (6)$$

where  $I(t)$  is the intensity decay (obtained at the magic angle),  $\otimes$  denotes convolution and  $L(t)$  the instrumental response function. The anisotropy decay was described by a sum of two exponentials (non-associative model), as follows:

$$\begin{aligned} r(t) &= (r_0 - r_\infty) \\ &[\beta_1 \exp(-t/\phi_1) + \beta_2 \exp(-t/\phi_2)] + r_\infty \end{aligned} \quad (7)$$

where  $r_0$  is the fundamental anisotropy. For Trp with excitation at 288 nm,  $r_0 = 0.173$ ; [22]) and was fixed during the analysis. This value of  $r_0$  with excitation at 288 nm corresponds to a local maximum in the polarization spectrum of Trp [22], and thus the error associated to the anisotropy decay analysis is minimized (namely, allowing the resolution of very fast components on the anisotropy decay). The

anisotropy parameters are more accurately recovered if a lesser number of parameters is optimized in the simultaneous fit [23]. In this way,  $\tau_i$  values obtained from the magic angle decay were kept fixed. The goodness of the fit was judged from the reduced  $\chi^2$  value, the random distribution of the weighted residuals, and the correspondence between the experimental steady-state value of anisotropy and the integrated anisotropy decay. The analysis of the data, in which each component of the magic angle fluorescence intensity decay was associated to one rotational correlation time (associative model), was also performed. However, no statistically meaningful parameters were recovered from such an analysis.

#### Other analytical procedures

Lipid concentration was determined by inorganic phosphorus analysis [24], and for Chol determination an enzymatic method (CHOD-PAP) was used [25,17].

### Results and discussion

#### *Trp<sup>6</sup> emission spectra and red-edge excitation shift: Trp-anchoring*

The absorption and fluorescence spectra of the  $\gamma$ M4 peptide incorporated in liposomes made of POPC/Chol 88:12 ( $l_d$  phase) and 55:45 mol:mol ( $l_o$  phase) MLV are shown in Figure 1. The absorption spectrum is independent of lipid composition. Regarding the emission, the spectral position was

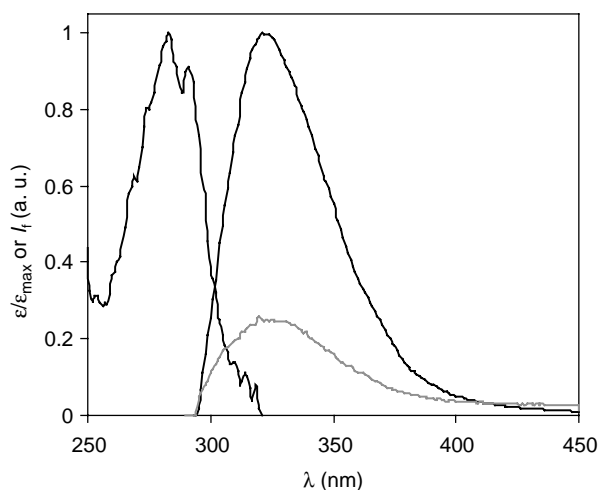


Figure 1. Absorption and emission ( $\lambda_{\text{excitation}} = 288$  nm) spectra of  $\gamma$ M4 in POPC/Chol 88:12 vesicles (black lines) and emission spectrum of  $\gamma$ M4 in POPC/Chol 55:45 (mol:mol) vesicles (gray line) at room temperature. The noise in the absorption spectrum is due to a maximum absorbance of  $\sim 0.05$  in a high scattering MLV suspension, an effect for which the spectrum had to be corrected. Peptide concentration is 0.7 mol% relative to total lipid.  $I_0$ : steady-state fluorescence intensity; a.u.: arbitrary units.

found to be insensitive to the presence of Chol, in agreement with recent results [26]. The emission maximum of  $\gamma$ M4 Trp<sup>6</sup> (corresponding to Trp<sup>453</sup> in the AChR sequence) in the lipid vesicles occurred at  $\lambda = 325$  nm. The significant blue-shift relative to an aqueous environment ( $\Delta\lambda = 25$  nm) clearly shows that Trp<sup>453</sup> is in a predominantly non-water solvating environment.

The REES effect of Trp<sup>6</sup> is shown in Figure 2. For Chol-rich vesicles, the quality of the data was poorer because, compared to the Chol-poor vesicles, both higher background light scattering and lower fluorescence intensity contributed adversely (Figure 1), and when exciting at the red-edge, the signal-to-noise ratio was too low to yield reliable data (not shown). The strong REES observed in the Chol-poor vesicles indicates: (i) a distribution of various solvated species in the ground state of the solute molecules (indole moiety [27]); (ii) polarity of the solvent; and (iii) relaxation of the solvent occurring more slowly or in competition with the solute fluorescence decay (according to [28] these are the three necessary conditions for the occurrence of a marked REES). The large blue-shift in the emission spectrum alone would be indicative of contact of Trp<sup>6</sup> with the lipid acyl chain region only. However, this would not lead to such a strong REES owing to the low polarity of the environment. It was previously concluded that Trp<sup>6</sup> is near the interface, probably very close to the carbonyl/first carbons of the acyl chain region of the phospholipid bilayer [17,26], as recently depicted by structural data [8]. The strong REES observed is in agreement with a Trp<sup>6</sup> location close to the membrane/water interface,

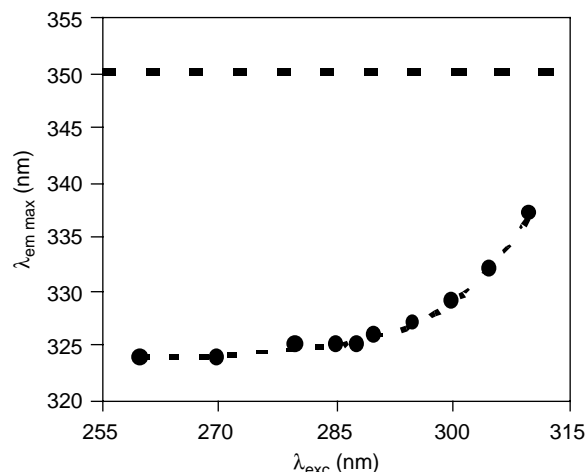


Figure 2. Red-edge excitation shift (REES) of the peptide  $\gamma$ M4 (Trp residue) incorporated in POPC vesicles. The dotted curve is merely a guide to the eye. The dashed line at 350 nm indicates the emission wavelength of Trp in aqueous solution and is shown for comparison. Peptide concentration is 3 mol% relative to total lipid.

where hydrogen bonding and steep polarity and/or dielectric changes may occur [27], indicating that the blue-shift alone is not sufficient to give in-depth information on Trp-containing peptides [29]. Furthermore, the precise location and rigidity of Trp<sup>6</sup> is in agreement with the concept of Trp-anchoring [30].

*Trp<sup>6</sup> time-resolved emission: decay-associated spectra and formation of peptide-rich patches*

The fluorescence decays of Trp<sup>6</sup> (Equation 1) could be described by a sum of three exponentials (reduced  $\chi^2 < 1.3$ ). In one of our previous studies [17] the lifetime-weighted quantum yields of the  $\gamma$ M4 peptide were studied at a single emission wavelength (340 nm) and at several concentrations, for both the  $l_d$  and  $l_o$  phases. Briefly, in the  $l_d$  phase, upon increasing the  $\gamma$ M4 peptide concentration from 0.7 mol% up to 7 mol%, the Trp lifetime-weighted quantum yield was halved. This could be accounted for by the presence of Cys and Lys residues in the  $\gamma$ M4 TM domain. Both Cys and Lys residues are known to be efficient quenchers of Trp fluorescence [31]. Thus, at high concentrations the proximity between  $\gamma$ M4 peptides leads to the diminution of Trp<sup>6</sup> intrinsic fluorescence owing to an intermolecular dynamic self-quenching process. For the  $l_o$  phase, the values for the lower concentrations (0.7 mol% and 3 mol%) in  $l_o$  are close to those found for the higher concentration in  $l_d$  (7 mol%). Since the dynamic self-quenching mechanism depends on the quencher concentration sensed by the fluorophore, in the case of  $\gamma$ M4 in Chol-rich vesicles there is a higher effective peptide concentration than expected from the analytical concentration. The diminution of the lifetime-weighted quantum yield

is reflected on the steady-state fluorescence intensity ( $I_F$ ), and thus in the emission spectra (Figure 1). Only a collisional mechanism is in the origin of the quenching, i.e., it is not revealing the presence of any permanent contacts. The effects of the collisional contribution of self-quenching on the fluorescence lifetime for a molecule with a complex decay were described by a modified Stern-Volmer equation [32] and allowed calculation of the lateral diffusion coefficient ( $D$ ) of the peptide in the Chol-poor membranes, showing an essentially random distribution of the peptide, i.e., with no evidence of inter-peptide interactions in the  $l_d$  phase [17].

In the present study, the fluorescence intensity decays were obtained for different emission wavelengths. All the decays (analysed individually) could be described by the sum of 3 exponentials (Equation 1), in which the lifetimes  $\tau_i$  were invariant, whereas the amplitudes  $\alpha_i$  presented a well defined and significant variation with emission wavelength. Based on this observation, the decays were analysed globally, forcing the lifetime of each component to be wavelength independent (linked). This allowed determination of the DAS (Equation 4), which are represented in Figure 3. When calculating DAS, it is implicit that the sample has different independent emissive species. In the present case, where only one fluorophore (Trp<sup>6</sup>) is present, this means that ground-state heterogeneity is assumed. The lifetime of each emissive species and the fractional area of its corresponding spectrum are given in Table I. Ground-state heterogeneity is supported by (see [33] and references therein) the complexity of the fluorescence decay of Trp in water and other low viscosity solvents, and of the Trp residue in small unstructured peptides in the same media, with a strong correlation observed between the amplitudes

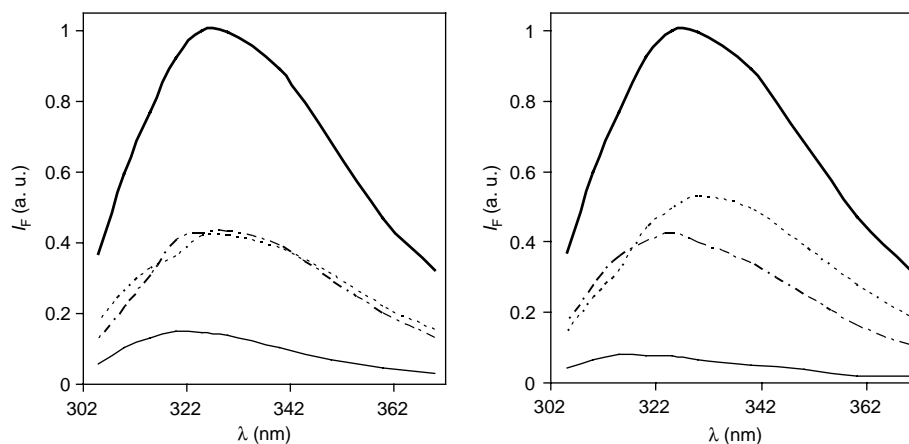


Figure 3. Decay-associated spectra (DAS) of the peptide  $\gamma$ M4 incorporated in Chol-rich ( $l_o$ , left panel) and Chol-poor ( $l_d$ , right panel) POPC vesicles obtained with  $\lambda_{\text{excitation}} = 288$  nm and at room temperature. The steady-state spectra are represented by a thick line. The other spectra correspond to the short (—), intermediate (---) and long lived (.....) emitting species shown in Table I. Peptide concentration is 0.7 mol% relative to total lipid.  $I_F$ : steady-state fluorescence intensity.

Table I. Fluorescence lifetime ( $\tau_i$ ) and fractional area contribution ( $A_i$ ) to the steady-state spectrum of each decay-associated spectra (DAS) of the Trp<sup>453</sup> residue in the  $\gamma$ M4 peptide incorporated into POPC/Chol vesicles with high ( $l_o$  phase) or low ( $l_d$  phase) Chol content at room temperature ( $\lambda_{exc} = 288$  nm). The concentration of  $\gamma$ M4 peptide is 0.7 mol% relative to total lipid.

Lipid phase	$\tau_1$ (ns)	$\tau_2$ (ns)	$\tau_3$ (ns)	$A_1$	$A_2$	$A_3$	$\chi^2$
$l_o$	0.24	1.29	5.19	0.13	0.43	0.44	1.5
$l_d$	0.43	2.42	5.94	0.07	0.41	0.52	1.3

of the fluorescence decay components and, for example, the circular dichroism spectra in the presence of growing amounts of  $\alpha$ -helix inducing solvent. The usual interpretation for the ground state heterogeneity is the existence of different ground-state rotamers that do not interconvert in the time-scale of the fluorescence lifetime ([33]; see also next paragraph). For example, the DAS and the corresponding centres of gravity are similar for both Trp and a 22-mer peptide related to REV-22, a regulator of HIV-1 expression [34]. Here, the multiple fluorescence lifetimes were also interpreted as originating from different rotameric states [35].

The global analysis (Table I) was statistically meaningful, as judged by the ratio of individual  $\chi^2$  from individual and global analysis, the global  $\chi^2$ , and the random distribution of residuals (not shown). DAS are a convenient way of representing a large set of results. The Trp photophysics is very complex [29], and both excited state relaxation and ground state heterogeneity can be present, and contribute to the appearance of the DAS, although the contribution of each effect cannot be discriminated completely [36]. However, in the present case the goal was to compare the behaviour of the DAS in  $l_d$  and  $l_o$ , respectively, which can be achieved. In addition to the wavelength invariance of the lifetimes obtained from individual analyses, other evidence points to ground-state heterogeneity as the main origin of the complexity of the fluorescence decay, namely: (i) the time-resolved emission spectra (not shown) have a complex contour that changes with time; (ii) there are no rise-time/negative pre-exponentials on any of the decays obtained; (iii) there is no correlation between the rotational correlation times (Equation 7; see next sub-section) and the fluorescence lifetimes corresponding to the DAS; and (iv) in the  $l_o$  phase the solvent relaxation is slower than in the  $l_d$  phase but the lifetimes are

shorter than in the  $l_d$  phase (the rotational dynamics are similar in both phases; see next sub-section).

The differences observed between the DAS in the  $l_d$  and in the  $l_o$  phases (Figure 3; Table I) are thus due to the intermolecular self-quenching that occurs in the  $l_o$  phase, due, in turn, to the formation of peptide-rich patches [17], as also observed directly by atomic force microscopy (AFM) for other peptides [37]. It is interesting that a similar change in the lifetime distribution was observed for a Trp-containing peptide interacting with membranes, but in this case the quencher was a lipid-like molecule inserted in the membrane [38]. In both cases, the secondary structure of the peptide was maintained, and different DAS were recovered due the occurrence of a quenching process.

#### *Time-resolved fluorescence anisotropy: $\gamma$ M4 nanosecond dynamics*

The steady-state anisotropy,  $\langle r \rangle$  (Table II), is insensitive to the presence of Chol, and reasonably high for a Trp-containing peptide, showing a strong immobilization. A comparison was made of these values with literature values from a systematic study of time-resolved anisotropy in which a single Trp was introduced at different positions along an  $\alpha$ -helical peptide in a fluid membrane [39]. After integration of the reported decays for peptides with the Trp residue not deeply buried in the hydrocarbon core of the bilayer [17], a value for the anisotropy of  $\langle r \rangle = 0.090 \pm 0.013$  was obtained, which is not significantly different from that obtained for the  $\gamma$ M4 peptide in the lipid vesicles (Table II).

The time-resolved fluorescence anisotropy decays for the  $\gamma$ M4 peptide in the  $l_d$  and in the  $l_o$  phases were also obtained (Figure 4). The parameters of Equation 7 describing the decays are given in Table

Table II. Time-resolved fluorescence anisotropy parameters of  $\gamma$ M4 (rotational correlation times  $\phi_i$ , amplitudes,  $\beta_i$ , and residual anisotropy  $r_\infty$ ) incorporated in Chol-rich ( $l_o$ ) and Chol-poor ( $l_d$ ) vesicles at room temperature. Also shown are the experimentally measured steady-state fluorescence anisotropy,  $\langle r \rangle_{exp}$ , and the steady-state anisotropy value calculated from integration of the anisotropy decay,  $\langle r \rangle_{calc}$ . Peptide concentration is 0.7 mol% relative to total lipid.

Lipid phase	$\langle r \rangle_{exp}$	$\phi_1$ (ns)	$\beta_1$	$\phi_2$ (ns)	$\beta_2$	$r_\infty$	$\chi^2$	$\langle r \rangle_{calc}$
$l_o$	$0.091 \pm 0.012$	$0.036 \pm 0.005$	$0.67 \pm 0.01$	$2.7 \pm 0.3$	$0.33 \pm 0.01$	$0.069 \pm 0.001$	1.5	$0.09 \pm 0.01$
$l_d$	$0.089 \pm 0.006$	$0.040 \pm 0.003$	$0.805 \pm 0.009$	$3.0 \pm 0.4$	$0.195 \pm 0.009$	$0.066 \pm 0.001$	1.3	$0.08 \pm 0.01$

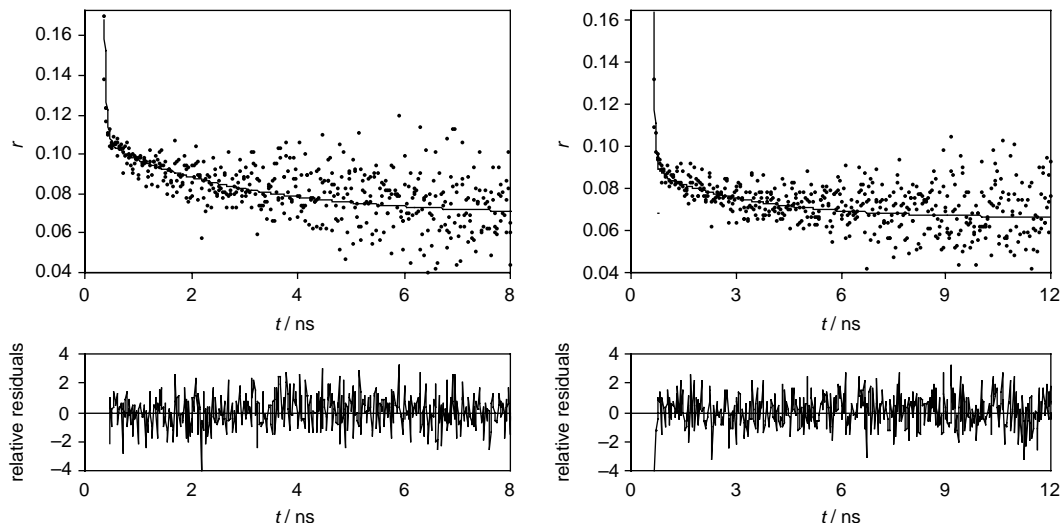


Figure 4. Time-resolved fluorescence anisotropy ( $r$ ) of Trp<sup>453</sup> of the peptide  $\gamma$ M4 incorporated in Chol-rich ( $l_o$ , left panel) and Chol-poor ( $l_d$ , right panel) POPC vesicles, obtained with excitation at 288 nm and emission at 340 nm. Top panels: the circles are experimental data points, and the solid lines are the corresponding fit of Eq. 7. Bottom panels: weighted residuals of each fit. The fitting parameters are given in Table II. Peptide concentration is 0.7 mol% relative to total lipid.

II. To see how well the recovered anisotropy parameters match with the experimentally determined steady-state anisotropy values, these values are compared with the calculated steady-state anisotropy from the integrated anisotropy decay (Table II). An agreement within  $<20\%$  is considered to be reasonably good on account of the large number of parameters involved [23]. In the present study, this figure always laid within  $<15\%$  (Table II).

No inter-peptide energy migration has been observed from steady-state anisotropy measurements [17], allowing inferences to be made about possible structures for the peptide aggregates. The similarity between the anisotropy decay parameters in  $l_d$  and  $l_o$  membranes reported here, further supports the absence of energy migration. An efficient energy migration due to parallel contacts would result in a stronger depolarization in the  $l_o$  phase. Hence, parallel dimers appear very improbable in the light of the present results, and more likely structures are peptide-rich patches without permanent contact, as observed in AFM imaging of other Lys-flanked peptides, [37] and anti-parallel aggregates as described for other Trp-flanked peptides [40]. Permanent aggregates, however would also lead eventually

to more notorious differences in the parameters describing the anisotropy decays.

The observed anisotropy decays were well described by two rotational correlation times,  $\phi_1$  and  $\phi_2$ , and a residual or limiting non-zero anisotropy in both Chol-poor and Chol-rich membranes (Figure 4, Table II). One rotational correlation time ( $\phi_1$ ) is very short and is the main contribution for depolarization. It is expected that  $\phi_1$  corresponds to the movement of the Trp<sup>6</sup> indole ring. The other one ( $\phi_2$ ) is  $\sim 3$  ns, contributes less to the fluorescence depolarization, and is expected to correspond to motions involving several amino acid residues. The limiting anisotropy at infinite time,  $r_\infty$ , makes a large contribution to the total anisotropy (Table II). Solute-solvent hydrogen bonding significantly hinders molecular rotation, and NH groups in the indole moiety are potentially capable of forming hydrogen bonds with the hydroxyl groups of surrounding molecules [23]. In this way, the hindered rotation, reflected in a high  $r_\infty$  value, further indicates strong interactions of the Trp<sup>6</sup> with the lipid C=O/phosphate backbone, even though the emission blue-shift alone would point to a hydrophobic environment. In addition to REES data

Table III. Parameters obtained from the application of an independent two-motion model (Eq. 8) to the fluorescence anisotropy decay of Trp<sup>6</sup> in  $\gamma$ M4 peptide incorporated in Chol-rich ( $l_o$ ) and Chol-poor ( $l_d$ ) vesicles at room temperature (order parameters,  $S_i$ , and semi-cone angles,  $\theta_i$ ), and diffusion coefficient ( $D_\perp$ ) corresponding to the backbone motion, and number of residues involved,  $n$ , in the motion being described. Peptide concentration is 0.7 mol% relative to total lipid.

Lipid phase	$\phi_{\text{indole}}$ (ns)	$\phi_{\text{backbone}}$ (ns)	$S_1$	$S_2$	$\theta_1$ ( $^\circ$ )	$\theta_2$ ( $^\circ$ )	$D_\perp$ ( $\text{s}^{-1}$ )	$n$
$l_o$	0.036	2.7	0.77	0.82	33	29	$14.4 \times 10^6$	12
$l_d$	0.040	3.0	0.71	0.87	38	24	$9.1 \times 10^6$	15

(Figure 2), the anisotropy decay indicates a strong anchoring of the peptide in the bilayer.

The two sets of rotational correlation times obtained ( $\phi_1$  and  $\phi_2$ ) differ from one another by more than one order of magnitude. Thus, according to a two-step model, the fast and slow motions are separable and the total correlation function is a product of the two correlation functions corresponding to the fast motion of the indole group and the slow motion of the peptide backbone [41]. The anisotropy decay is then described by:

$$r(t) = r_0 [(1-S_1^2)\exp(-t/\phi_{\text{indole}}) + (1-S_2^2)S_1^2\exp(-t/\phi_{\text{backbone}}) + S_1^2S_2^2] \quad (8)$$

where  $S_1$  and  $S_2$  are the order parameters corresponding to  $\phi_1$  and  $\phi_2$ , respectively. Owing to the large difference between the observed rotational correlation times, this equation is equivalent to Equation 7 making  $\phi_1 \approx \phi_{\text{indole}}$ ,  $\phi_2 \approx \phi_{\text{backbone}}$ ,  $\beta_1 = 1-S_1^2$ ,  $\beta_2 = 1-S_2^2$  and  $r_\infty/r_0 = S_1^2S_2^2$ . According to the wobbling-in-cone model, the order parameters allow calculation of the semi-angle  $\theta$  of the cone where the movement is free to occur [42]. The order parameter and the semi-angle of the cone are related through  $\cos \theta_i = 1/2[(8S_i + 1)^{1/2} - 1]$ , and the values calculated for  $\gamma\text{M4}$  in  $l_d$  and  $l_o$  phases are listed in Table III. As was already apparent from Table II, the rotational dynamics of the peptide are similar in both lipid phases (not surprisingly, because both are fluid lipid bilayers). However, significant differences in each parameter were found, as shown in Table III.

The two-step model in conjunction with the wobbling-in-cone model had been successfully applied to the calculation of dynamical properties of fluorescent molecules in micellar systems (e.g., [23], and references therein). In the case of tyrosine or tryptophan containing peptides, assuming that the TM domain behaves as a rigid body in the bilayer, it is possible to estimate the diffusion coefficient ( $D_\perp$ ) corresponding to the rigid body fluctuations from the longest rotational correlation time, which was used to calculate the dimension and number of amino acid residues involved in the movement of the potassium channel inhibitor shaker B peptide [43]. For cylindrical rotors, the friction coefficient is only dependent on the length-to-diameter ratio, making this method most suitable for estimating segments in cylindrically shaped peptides. In the case of the Shaker B peptide, the intrinsic tyrosine fluorescence allowed estimation of the segment size with the expected number of residues involved from other techniques [43]. In case of  $\gamma\text{M4}$  peptide, the fluorescence of Trp is used, which occurs at longer wavelengths than that of tyrosine, which is advantageous in membrane studies. Assuming that the peptide presents an  $\alpha$ -helical structure (see Intro-

duction), it can be modelled as a cylinder with diameter 10 Å [44], with length corresponding to  $1.5 \text{ \AA} \times n$  (the number of residues involved in the movement reflected in  $\phi_{\text{backbone}}$ ). Thus, the volume occupied by the helix segment is directly related to the number of amino acid residues ( $n$ ) in that segment. By calculating the value of  $D_\perp$  that would be obtained for helical segments with different lengths, and comparing it with the value extracted from the anisotropy decay (Table III), it is possible to determine  $n$ . The results of these calculations are shown in Table III.

From Table III, motions described by  $\phi_2$  and hence,  $S_2$ , involve 15 residues in the  $l_d$  phase and 12 residues in the  $l_o$  phase. Considering that the cytoplasmic-located moiety of the  $\gamma\text{M4}$  peptide [8] is strongly anchored to the membrane (through both Lys<sup>2</sup> and Trp<sup>6</sup>; [45] and results presented here), the helical segment with backbone motion described by  $\phi_2$  and  $S_2$  corresponds approximately to the sequence 451 to 451 +  $n$  (in the  $\gamma$  subunit). In the case of  $l_o$  phase, this segment ends near the central Gly<sup>462</sup>. Thus, in the timescale of fluorescence emission, the segment 451 to 451 +  $n$  would behave as a rigid body. The peptide would not have a defined kink (for which a Pro residue is necessary), but a moderately higher degree of flexibility near the centre of the bilayer. It should be noted that the movement described is very fast (within a few ns) and restricted, and would be averaged by most other techniques, namely NMR and cryoelectron microscopy, being thus compatible to the general description of the TM portion of  $\gamma\text{M4}$  alone or in the whole receptor as a straight  $\alpha$ -helix [8,26]. In fact, fluorescence spectroscopy is unique in detecting molecular motions in the nanosecond time-scale [42]. In a recent NMR study of the reconstituted peptide, no significant flexibility was detected between Ala<sup>8</sup> and Gly<sup>15</sup> [46]. For the peptide embedded in the  $l_d$  phase, the movement sensed by the Trp anchor would entail a greater proportion of the helix (15 residues).

The rotational correlation times obtained here indicate that the multiple fluorescence lifetimes arise mainly from different rotameric states. In studies of the peptide REV22 [35] it was argued that the longer rotational correlation time obtained (1.5 ns) is in fact close to that expected if the peptide were considered a sphere (0.90 ns). The short 155 ps rotational correlation time is much shorter than that obtained for other single Trp proteins: a  $\sim 500$  ps 'fast' rotational correlation time is observed for several single-Trp proteins studied [47], where it is reasoned that the  $\sim 500$  ps isotropic lifetime originates from spectral relaxation that is induced by 'fast' structural dynamics reflected in the  $\sim 500$  ps

rotational correlation time. The short rotational correlation time found here (Table III) is much faster than the isotropic  $\sim 500$  ps component discussed previously [49] and no correlation between  $\tau_1$  and  $\phi_1$  is apparent in our data. The long rotational correlation time ( $\phi_2$ ) could be explained as peptide backbone fluctuations. Similar features that favour rotameric origin of multi-exponentiality for REV22 peptide are observed for melittin [48]. Again, as observed here for  $\gamma$ M4 in  $l_d$  and  $l_o$  lipid phases, different amplitude for the lifetimes, but the same position of the steady-state emission spectra and same rotational correlation times, were observed in the case of melittin in different aqueous media [48], once again favouring the rotamer interpretation of the origin of the multi-exponentiality. Here, for the  $\gamma$ M4 peptide, solvent relaxation mechanisms are probably present and contribute to the observed fluorescence decay, but whereas ground-state heterogeneity is undoubtedly present, evidence of solvent relaxation (rise time/negative pre-exponential, TREES with shift but no shape change [49]) was not observed.

#### *Implications for the dynamics and function of the whole acetylcholine receptor*

From a recent MD simulation study of the TM portion of the receptor [10], in which, at time zero, each M4 helix was positioned at  $\sim 20^\circ$ , for  $\gamma$ M4, the tilt angle reached a value of  $\sim 27^\circ$  within 3 ns and fluctuated around this value during the rest of the simulation. Also, approximately 16% of the  $\alpha$ -helicity of the M4 segments was lost at 35 ns with respect to the starting structure; the partial loss of the  $\alpha$ -helicity occurred not only at the extremities but also within some TM segments. The  $\alpha$ -helix bend or turn switch within the TM segment led to the formation of flexible hinges within the helix. Additionally, the M4 segments increase their hydrophobic interactions with the surrounding dipalmitoylphosphatidylcholine molecules by burying themselves deeper into the hydrophobic region of the bilayer, and the interactions of the M4 ring with the inner M1-M3 TM portion and with the lipid molecules, respectively, suggest that the outer ring of M4 acts as the vehicle to transfer the influence of the lipid surroundings to the conformation changes of the whole AChR [10].

In the present study, the flexibility of the  $\gamma$ M4 helix approximately halfway through its hydrophobic length was experimentally verified in Chol-rich membranes. This may be related to the structural alterations suggested by the MD study [10]. It is worth noting that both phenomena are in the ns timescale, and thus are averaged by most other

techniques. This flexibility is important for helix-helix interactions, since Gly<sup>462</sup> and Thr<sup>463</sup> are approximately in the middle of the  $\gamma$ M4 helix, and both have small side chains, facilitating close packing of helices and perhaps being involved in the transmission of changes in lipid environment to the M1-M3 pore-forming sector of the channel through the M4 outer ring in direct contact with the lipid milieu [2,10]. As mentioned in the Introduction, M4 helices do not contact with each other in the whole protein. Here we verify that there is a significant difference in the dynamics of the peptide in the  $l_d$ , and in the  $l_o$  phase, but this difference is not dramatic.

There are different contributions to the free energy of insertion of TM peptides in the lipid bilayer, and though the overall result is a negative free energy, there are positive contributions [50]. This penalty should be higher in the  $l_o$  than the  $l_d$  phase, and usually TM peptides partition preferentially to the  $l_d$  phase [51]. Nevertheless, native AChR-rich membranes are particularly rich in Chol, and Chol is known to stabilize the structure and functionality of the AChR protein (see [2,3]), thus the interactions in the Chol-rich phase should mimic the interactions in the native membrane better than in the Chol-poor phase. Even though the peptide aggregates in the  $l_o$  phase, it retains a similar dynamics and flexibility as in the  $l_d$  phase. This suggests that the peptide-rich patches formed in Chol-rich phases are mainly dynamic aggregates without permanent contacts (antiparallel contacts cannot be ruled out). Nevertheless, the fine difference in the dynamics of the peptide between the two phases could be related to the stabilizing effect of cholesterol on the receptor. Recent data [26] indicate a higher degree of tilting of the peptide in  $l_d$  phase compared to  $l_o$  or gel-phase bilayers. The tilt angle found for the thicker bilayers is close to that for the native receptor ( $\sim 20^\circ$ ; [8]) which favours helix-helix interactions. In the absence of Chol, tilt angles higher than  $30^\circ$  prevent the close-packing of the helices at approximately the center of the bilayer, and reduce the macrodipole-macrodipole attraction, leading to a preponderance of the lipid-peptide interactions, a condition which could prevent the proper assembly of the receptor. In this way, one should not expect a priori that the value of  $n$  should be higher for the peptide in the  $l_o$  phase than in the  $l_d$  phase, because not only the lipid phase changes, but also lipid-peptide and peptide-peptide interactions are different, and in fact the value found for  $l_d$  does not point to any specific peptide-peptide interaction (around Ala<sup>18</sup>) whereas the one in  $l_o$  does.

The interfacial part of the  $\gamma$ M4 peptide containing Trp<sup>6</sup> (and Lys<sup>2</sup>) is strongly anchored and immobile,

as shown by the very high value of the limiting anisotropy and the order parameter  $S_1$ . Thus it is interesting to hypothesize on a possible role for the severe rotational restriction of Trp<sup>453</sup> (and probably the nearby residues including Lys<sup>449</sup>). We suggest that this restriction optimizes specific interactions of the receptor at the level of the phospholipid headgroup. It is known that phosphatidic acid (PA), a monoanionic phospholipid at neutral pH, has a higher affinity for the vicinity of the AChR than either neutral lipids such as PC or anionic ones as phosphatidylglycerol or phosphatidylserine with the same acyl chains [52]. The presence of positively charged residues at the end of the M4 TM segments, i.e., at the level of the phospholipid headgroup, has been pointed out [5,53]. It has also been suggested that the initial interaction of PA with the receptor protein is mainly electrostatic [54], and that competition between Chol and palmitoyl-oleoyl-PA for the same binding sites on the AChR protein probably occurs [54]. Altogether, these studies point to a probable role of the  $\gamma$ M4 region of the protein in its interaction with PA. However, the molecular details responsible for the preference for a certain anionic lipid in detriment of the others remain unknown. In one of the previously mentioned studies, it is pointed out that the selectivity must be determined by subtle molecular details of the interaction between the entire phospholipid headgroup and specific sites in the AChR [54]. Thus, it is suggested here that the Lys-Trp anchor of the  $\gamma$ M4 peptide, owing to its rigidity, is able to optimize its interaction only with PA, and not other classes of anionic phospholipid headgroups.

### Acknowledgements

We would like to thank Fundação para a Ciência e a Tecnologia, Portugal, for financing research projects and R. F. M. de A.'s and A. F. post-doc grants (SFRH/BPD/17842/2004 and 11488/2002) under the program POCTI. This work was supported in part by grants from the Universidad Nacional del Sur, the Agencia Nacional de Promoción Científica (FONCYT), Argentina, and FIRCA 1-RO3-TW01225-01 (NIH) to F. J. B., and a grant from the MRC (UK) to A. W.

### References

- [1] Corringer PJ, Le Novère N, Changeux JP. Nicotinic receptors at the amino acid level. *Ann Rev Pharmacol Toxicol* 2000;40:431–458.
- [2] Barrantes FJ. Transmembrane modulation of nicotinic acetylcholine receptor function. *Curr Opin Drug Disc Develop* 2003;6:620–632.
- [3] Barrantes FJ. Structural basis for lipid modulation of nicotinic acetylcholine receptor function. *Brain Res Rev* 2004;47:71–95.
- [4] Marsh D, Barrantes FJ. Immobilized lipid in acetylcholine receptor-rich membranes from *Torpedo marmorata*. *Proc Natl Acad Sci USA* 1978;75:4329–4333.
- [5] Blanton MP, Cohen JB. Mapping the lipid-exposed regions in the *Torpedo californica* nicotinic acetylcholine receptor. *Biochemistry* 1992;31:3738–3750.
- [6] Blanton MP, Cohen JB. Identifying the lipid-protein interface of the *Torpedo* nicotinic acetylcholine receptor: secondary structure implications. *Biochemistry* 1994;33:2859–2872.
- [7] Blanton MP, Xie Y, Dangott LJ, Cohen JB. The steroid promegestone is a noncompetitive antagonist of the *Torpedo* nicotinic acetylcholine receptor that interacts with the lipid-protein interface. *Mol Pharmacol* 1999;55:269–278.
- [8] Miyazawa A, Fujiyoshi Y, Unwin N. Structure and gating mechanism of the acetylcholine receptor pore. *Nature* 2003;423:949–955.
- [9] Watts A. Solid-state NMR in drug design and discovery for membrane-embedded targets. *Nat Rev Drug Discov* 2006;5:555–568.
- [10] Xu Y, Barrantes FJ, Luo X, Chen K, Shen J, Jiang H. Conformational dynamics of the nicotinic acetylcholine receptor channel: A 35-ns molecular dynamics simulation study. *J Am Chem Soc* 2005;127:1291–1299.
- [11] Tamamizu S, Guzman GR, Santiago J, Rojas LV, McNamee MG, Lasalde-Dominicci JA. Functional effects of periodic tryptophan substitutions in the  $\gamma$ M4 transmembrane domain of the *Torpedo californica* nicotinic acetylcholine receptor. *Biochemistry* 2000;39:4666–4673.
- [12] Lee YH, Li L, Lasalde J, Rojas L, McNamee MG, Ortiz-Miranda SI, Pappone P. Mutations in the M4 domain of *Torpedo californica* acetylcholine receptor dramatically alter ion channel function. *Biophys J* 1994;66:646–653.
- [13] Bouzat C, Roccamo AM, Garbus I, Barrantes FJ. Mutations at lipid-exposed residues of the acetylcholine receptor affect its gating kinetics. *Mol Pharmacol* 1998;54:146–153.
- [14] daCosta CJ, Ogrel AA, McCardy EA, Blanton MP, Baenziger JE. Lipid-protein interactions at the nicotinic acetylcholine receptor. A functional coupling between nicotinic receptors and phosphatidic acid-containing lipid bilayers. *J Biol Chem* 2002;277:201–208.
- [15] de Almeida RFM, Fedorov A, Prieto M. Sphingomyelin/phosphatidylcholine/cholesterol phase diagram: boundaries and composition of lipid rafts. *Biophys J* 2003;85:2406–2416.
- [16] Gill SC, von Hippel PH. Calculation of protein extinction coefficients from amino acid sequence data. *Anal Biochem* 1989;182:319–326.
- [17] de Almeida RFM, Loura LMS, Prieto M, Watts A, Fedorov A, Barrantes FJ. Cholesterol modulates the organization of the  $\gamma$ M4 transmembrane domain of the muscle nicotinic acetylcholine receptor. *Biophys J* 2004;86:2261–2272.
- [18] Chen RF. Fluorescence quantum yields of tryptophan and tyrosine. *Anal Lett* 1967;1:35–42.
- [19] Loura LMS, Fedorov A, Prieto M. Resonance energy transfer in a model system of membranes: Application to gel and liquid crystalline phases. *Biophys J* 1996;71:1823–1836.
- [20] Lakowicz JR. Principles of fluorescence spectroscopy, 2nd ed. New York: Kluwer/Plenum; 1999.
- [21] Knutson JR, Beechem JM, Brand L. Simultaneous analysis of multiple fluorescence decay curves – a global approach. *Chem Phys Lett* 1983;102:501–507.

- [22] Valeur B, Weber G. Resolution of the fluorescence excitation spectrum of indole into the  $^1\text{La}$  and  $^1\text{Lb}$  excitation bands. *Photochem Photobiol* 1977;25:441–444.
- [23] Dutt GB. Rotational diffusion of nondipolar probes in Triton X-100 micelles: Role of specific interactions and micelle size on probe dynamics. *J Phys Chem B* 2002;106:7398–7404.
- [24] McClare CWF. An accurate and convenient organic phosphorus assay. *Anal Biochem* 1971;39:527–530.
- [25] Deeg R, Ziegenhorn J. Kinetic enzymatic method for automated determination of total cholesterol in serum. *Clin Chem* 1983;29:1798–1802.
- [26] Antollini SS, Xu Y, Jiang H, Barrantes FJ. Fluorescence and molecular dynamics studies of the acetylcholine receptor  $\gamma\text{M4}$  transmembrane peptide in reconstituted systems. *Mol Membr Biol* 2005;22:471–483.
- [27] Chattopadhyay A, Raghuraman H. Application of fluorescence spectroscopy to membrane protein structure and dynamics. *Curr Sci* 2004;87:175–180.
- [28] Itoh KI, Azumi T. Shift of emission band upon excitation at long wavelength absorption-edge 2. Importance of solute-solvent interaction and solvent reorientation relaxation process. *J Chem Phys* 1975;62:3431–3438.
- [29] de Almeida RFM, Loura LMS, Prieto M. Application of fluorescence to understand the interaction of peptides with binary lipid membranes. *Rev Fluorescence* 2005;2:271–323.
- [30] Ridder ANJA, Morein S, Stam JG, Kuhn A, de Kruijff B, Killian JA. Analysis of the role of interfacial tryptophan residues in controlling the topology of membrane proteins. *Biochemistry* 2000;39:6521–6528.
- [31] Chen Y, Barkley MD. Toward understanding tryptophan fluorescence in proteins. *Biochemistry* 1998;37:9976–9982.
- [32] Sillen A, Engelborghs Y. The correct use of ‘average’ fluorescence parameters. *Photochem Photobiol* 1998;67:475–486.
- [33] Dahms TES, Szabo AG. Probing local secondary structure by fluorescence: Time-resolved and circular dichroism studies of highly purified neurotoxins. *Biophys J* 1995;69:569–576.
- [34] Kingsman SM, Kingsman AJ. The regulation of human immunodeficiency virus type-1 gene expression. *Eur J Biochem* 1996;240:491–507.
- [35] Larsen OFA, van Stokkum IHM, Pandit A, van Grondelle R, van Amerongen H. Ultrafast polarized fluorescence measurements on tryptophan and a tryptophan-containing peptide. *J Phys Chem B* 2003;107:3080–3085.
- [36] Ladokhin AS. On the interpretation of decay-associated fluorescence spectra in proteins. *Biopolymers Cell* 2001;17:221.
- [37] Rinia HA, Boots JWP, Kik RA, Snel MME, Demel RA, Killian JA, van der Erden JPJM, de Kruijff B. Domain formation in phosphatidylcholine bilayers containing transmembrane peptides: Specific effects of flanking residues. *Biochemistry* 2002;41:2814–2824.
- [38] de Foresta B, Tortech L, Vincent M, Gallay J. Location and dynamics of tryptophan in transmembrane alpha-helix peptides: A fluorescence and circular dichroism study. *Eur Biophys J* 2002;31:185–198.
- [39] Vogel H, Nilsson L, Rigler R, Vogues KL, Jung G. Structural fluctuations of a helical polypeptide traversing a lipid bilayer. *Proc Natl Acad Sci USA* 1988;85:5067–5071.
- [40] Sparr E, Ganchev DN, Snel MME, Ridder ANJA, Kroon-Batenburg LMJ, Chupin V, Rijkers DTS, Killian JA, de Kruijff B. Molecular organization in striated domains induced by transmembrane  $\gamma$ -helical peptides in dipalmitoyl phosphatidylcholine bilayers. *Biochemistry* 2005;44:2–10.
- [41] Lipari G, Szabo A. Effect of vibrational motion on fluorescence depolarization and nuclear magnetic resonance relaxation in macromolecules and membranes. *Biophys J* 1980;30:489–506.
- [42] Kinosita K Jr, Kawato S, Ikegami A. A theory of fluorescence polarization decay in membranes. *Biophys J* 1977;20:289–305.
- [43] Poveda JA, Prieto M, Encinar JA, Gonzalez-Ros JM, Mateo CR. Intrinsic tyrosine fluorescence as a tool to study the interaction of the Shaker B ‘Ball’ peptide with anionic membranes. *Biochemistry* 2003;42:7124–7132.
- [44] Bowie JU. Helix packing in membrane proteins. *J Mol Biol* 1997;272:780–789.
- [45] de Planque MR, Kruijtz JA, Liskamp RM, Marsh D, Greathouse DV, Koeppe 2nd RE, de Kruijff B, Killian JA. Different membrane anchoring positions of tryptophan and lysine in synthetic transmembrane alpha-helical peptides. *J Biol Chem* 1999;274:20839–20846.
- [46] Williamson PTF, Zandomeneghi G, Barrantes FJ, Watts A, Meier BH. Structural and dynamic studies of the  $\gamma$ -M4 transmembrane domain of the nicotinic acetylcholine receptor. *Mol Membr Biol* 2005;22:485–496.
- [47] Lakowicz JR. On spectral relaxation in proteins. *Photochem Photobiol* 2000;72:421.
- [48] Pandit A, Larsen OFA, van Stokkum IHM, van Grondelle R, Kraayenhof R, van Amerongen H. Ultrafast polarized fluorescence measurements on monomeric and self-associated melittin. *J Phys Chem B* 2003;107:3086–3090.
- [49] Toptygin D, Savtchenko RS, Meadow ND, Brand L. Homogeneous spectrally- and time-resolved fluorescence emission from single-tryptophan mutants of IIA<sup>Glc</sup> Protein. *J Phys Chem B* 2001;105:2043–2055.
- [50] Lundbaek JA, Anderson OS, Werge T, Nielsen C. Cholesterol-induced protein sorting: An analysis of energetic feasibility. *Biophys J* 2003;84:2080–2089.
- [51] Vidal A, McIntosh TJ. Transbilayer peptide sorting between raft and nonraft bilayers: Comparisons of detergent extraction and confocal microscopy. *Biophys J* 2005;89:1102–1108.
- [52] Poveda JA, Encinar JA, Fernandez AM, Mateo CR, Ferragut JA, Gonzalez-Ros JM. Segregation of phosphatidic acid-rich domains in reconstituted acetylcholine receptor membranes. *Biochemistry* 2002;41:12253–12262.
- [53] Noda M, Takahashi H, Tanabe T, Toyosato M, Kikyotani S, Furutani Y, Hirose T, Takashima H, Inayama S, Miyata T, Numa S. Structural homology of *Torpedo californica* acetylcholine receptor subunits. *Nature* 1983;302:528–532.
- [54] Wenz J, Barrantes FJ. Nicotinic acetylcholine receptor induces lateral segregation of phosphatidic acid and phosphatidylcholine in reconstituted membranes. *Biochemistry* 2005;44:398–410.